Electronic Supplementary Information

Elucidating Metal and Ligand Redox Activities of Copper-Benzoquinoid Coordination Polymer as Cathode for Lithium-Ion Batteries

Cheng-Han Chang,[a,‡] An-Che Li,[bc,‡] Ilja Popovs,[d] Watchareeya Kaveevivitchai,[bc] Jeng-Lung Chen,[e] Kai-Chun Chou,[a] Ting-Shen Kuo,[f] and Teng-Hao Chen*[g]

[a.] Department of Chemistry, Tamkang University, New Taipei City 25137, Taiwan

[b.] Department of Chemical Engineering, National Cheng Kung University, Tainan City 70101, Taiwan

[c.] Hierarchical Green-Energy Materials Research Center, National Cheng Kung University, Tainan City 70101, Taiwan

[d.] Chemical Sciences Division, Oak Ridge National Laboratory, Oak Ridge, P.O. Box 2008, TN 37831, USA

[e.] National Synchrotron Radiation Research Center, Hsinchu 30076, Taiwan

[f.] Department of Chemistry, National Taiwan Normal University, Taipei 11677, Taiwan

[g.] School of Pharmacy, National Cheng Kung University, Tainan City 70101, Taiwan

‡These authors contributed equally to this work.

*To whom correspondence should be addressed. E-mail: thchen@gs.ncku.edu.tw

General methods and materials

Starting materials and solvents were purchased and used without further purification from commercial suppliers (Sigma-Aldrich and TCI). ^{1}H and ^{13}C nuclear magnetic resonance (NMR) spectra were recorded on a Bruker AV300 or AV600 spectrometer. Chemical shifts are quoted in parts per million (ppm) referenced to the appropriate solvent peak. Fourier-transform infrared (FT-IR) spectra were recorded on Nicolet iS5 or Nicolet 6700, Thermo Scientific. Powder X-ray diffraction (PXRD) patterns were collected on Bruker D8 Advance. Single-crystal X-ray diffraction experiments were performed by using Bruker D8 Venture dual X-ray single crystal diffractometer. Thermogravimetric analyses (TGA) were carried out on a TA Instrument TGA 2050 from 25 to 900 °C with a ramping rate 20 °C min^{-1} under the flow of N_2. Mass spectrometry measurements were recorded on Bruker Autoflex III TOF/TOF system MALDI MASS. Cyclic voltammetry (CV) experiments were performed in solution using a CH Instruments Electrochemical Analyzer. All measurements were carried out at room temperature with a conventional three-electrode configuration consisting of a carbon working electrode, a platinum wire auxiliary electrode, and a Ag/AgCl reference electrode. X-ray absorption spectroscopy experiments were performed at beamline TPS44A at National Synchrotron Radiation Research Center, Hsinchu, Taiwan. X-ray photoelectron spectroscopy (XPS) measurements were done using ULVAC PHI 5000 VersaProbe Ⅲ equipped with an Al Kα (1487 eV) as a radiation source. Survey scans were collected with a pass energy of 100 eV, followed by a high-resolution scans of the C 1s and Cu 2p regions with a pass energy of 20 eV. All spectra were charge-corrected relative to the C 1s component at 284.7 eV binding energy, and analyzed using CasaXPS software. High-resolution transmission electron microscopy (HR-TEM) was carried out on JEM-2010 Electron Microscope, JEOL. Elemental analysis was performed on Elementar Vario EL III.

Electrochemical characterization

Coordination polymer (CP) crystals were mixed and ground with carbon black (CB, Super P), graphite (TIMREX® KS4), and poly(vinylidenedifluoride) (PVDF) in *N*-methyl-2-pyrrolidinone (NMP) in a 3:5:1:1 weight ratio. The slurry was coated onto carbon paper (EP40) current collector. The electrodes were dried overnight at 100 °C in vacuum. LH_4 electrodes were prepared with the same additives as a comparison with CP electrodes. CR2032 coin cells were assembled by using Li metal anode, 1 M $LiPF_6$ in 1:1 v/v ethylene carbonate (EC)/ dimethyl carbonate (DMC) electrolyte solution, and Celgard separator. The electrochemical testing was carried out with an Arbin cycler and a VMP3 system (BioLogic) at various current densities. Galvanostatic intermittent

titration technique (GITT) was performed by alternating 20 mA g^{-1} pulses (30 min) with relaxation periods (90 min).

Synthesis of 2, 3, 5, 6-tetra-*tert*-butoxyterephthalonitrile

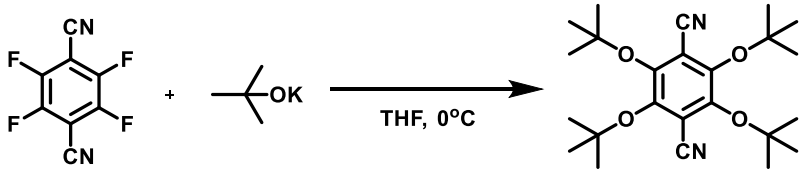

Solid potassium *tert*-butoxide (30.3 g, 270 mmol) was placed in a 1000 mL round bottom flask equipped with a magnetic stir bar, and 270 mL of anhydrous tetrahydrofuran (THF) was added via cannula under nitrogen atmosphere. After stirring for 20 min, the resulting solution was cooled to 0 °C using ice bath, and the solution of tetrafluorobenzodinitrile (12.0 g, 60 mmol) in 30 mL of anhydrous THF was slowly added via syringe (CAUTION: EXOTHERMIC REACTION !!!), upon addition the color of the reaction mixture changes from colorless to dark yellow. After complete addition of dinitrile, the reaction mixture was allowed to warm up to room temperature, and allowed to stir for 1 h. The reaction mixture was cooled back with an ice bath, and 600 mL of deionized water was added to the vigorously stirred reaction mixture, causing the intermediate product to precipitate. The precipitate was filtered off, and washed with the additional amount of 3×300 mL of deionized water/methanol mixture 1:1 v/v. The resulting white solid was air- and vacuum-dried overnight and used in the next step without further purification. Yield: 90%. ^{1}H NMR (600MHz, $CDCl_3$): δ 1.43 (CH_3). ^{13}C NMR (600MHz, $CDCl_3$) δ 29.15, δ 87.34, δ 115.65, δ 115.70, δ 149.73. FT-IR: 2977 (s, $\tilde{\nu}_{C-H}$), 2231 (s, $\tilde{\nu}_{C\equiv N}$), 1262 (s, $\tilde{\nu}_{C-O}$). MALDI-TOF (m/z) $[M+H]^+$ calculated for $C_{24}H_{36}N_2O_4$, 416.27, found 417.31.

Synthesis of 1,4-dicyano-2,3,5,6-tetrahydroxybenzene (LH_4)

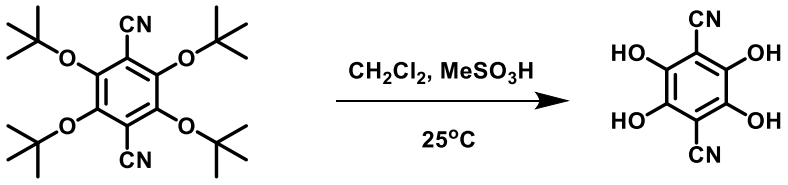

2, 3, 5, 6-tetra-*tert*-butoxyterephthalonitrile (13.8 g, 33.1 mmol) was dissolved in 120 mL of dichloromethane (DCM). To this solution, 6 mL of methane sulfonic acid ($MeSO_3H$) was slowly added, causing the precipitation of the product. The reaction mixture was vigorously stirred for 12 h at 25 °C, after which the product was filtered off and washed with the additional amount of DCM 3×100 mL, air-dried and finally dried under high vacuum to afford product. Yield: 75%. ^{1}H NMR (600MHz, d_6-DMSO): δ 9.88 (OH). ^{13}C NMR (600MHz, d_6-DMSO) δ 97.77, δ 114.06, δ 141.07. FT-IR:

3419 (s, $\tilde{\nu}_{O-H}$), 2245 (s, $\tilde{\nu}_{C\equiv N}$). MALDI-TOF (m/z) $[M+H]^+$ calculated for $C_8H_4N_2O_4$, 192.13, found 192.95.

Synthesis of coordination polymer $[CuL(DMF)_2]_n$

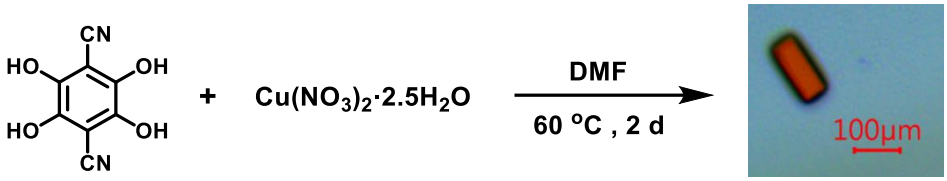

LH_4 (20 mg, 0.1 mmol) and $Cu(NO_3)_2{\cdot}3H_2O$ (20 mg, 0.1mmol) were dissolved in 30 mL of *N,N*-dimethylformamide (DMF). The solution was transferred into a 4 mL vial and heated at 60 °C for 48 h. The reaction product was cooled to room temperature and afforded orange single crystals. The product was washed with DMF (3×5 mL) and ethyl acetate (3×5 mL) and dried in vacuum at 70 °C for 8 h. Yield calculated from the evacuated sample was 68 % based on Cu. FT-IR: 2215 (s, $\tilde{\nu}_{C\equiv N}$), 1655 (s, $\tilde{\nu}_{C=O}$). Anal. calcd (%) for $CuC_{14}H_{14}N_4O_6$: C 42.25, H 3.55, N 14.08; Found: C 41.21, H 2.88, N 13.70.

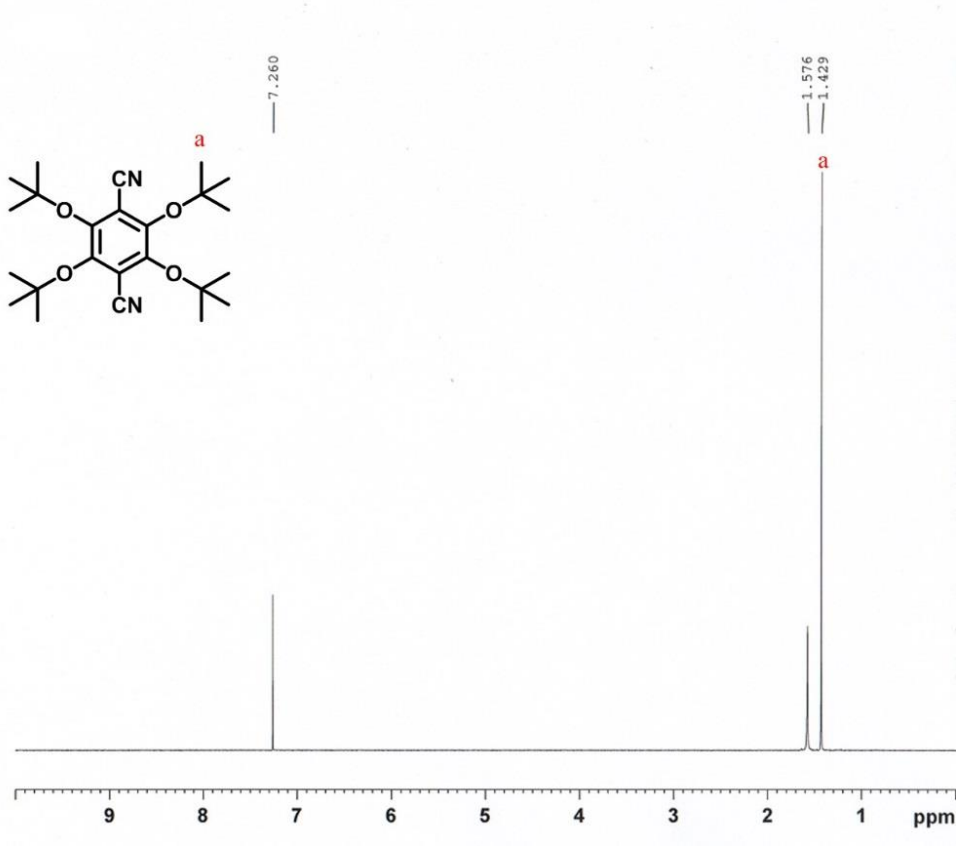

Fig. S1 ^{1}H NMR spectrum of 2, 3, 5, 6-tetra-*tert*-butoxyterephthalonitrile.

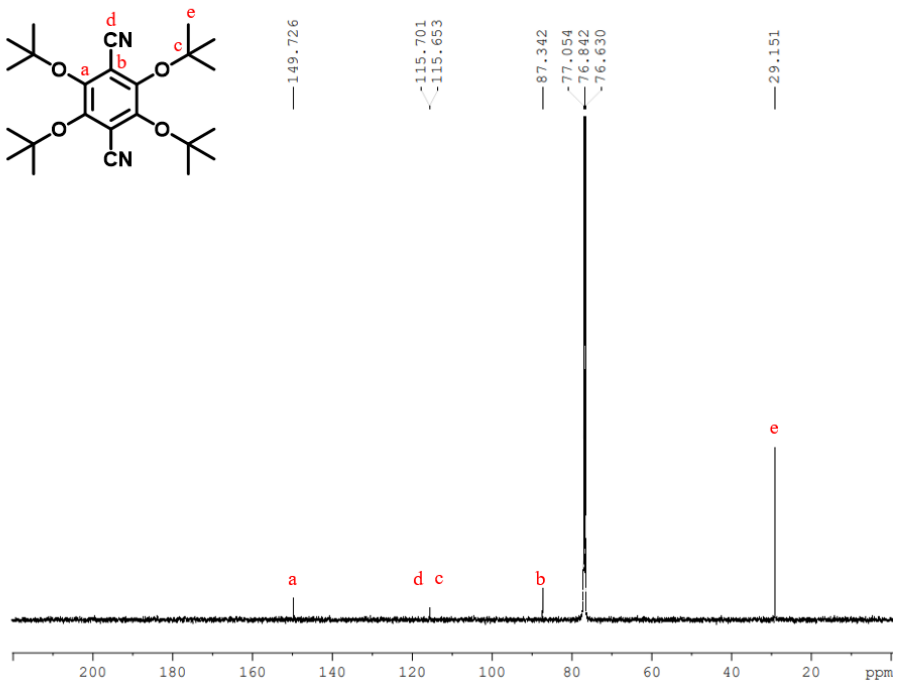

Fig. S2 ^{13}C NMR spectrum of 2, 3, 5, 6-tetra-*tert*-butoxyterephthalonitrile.

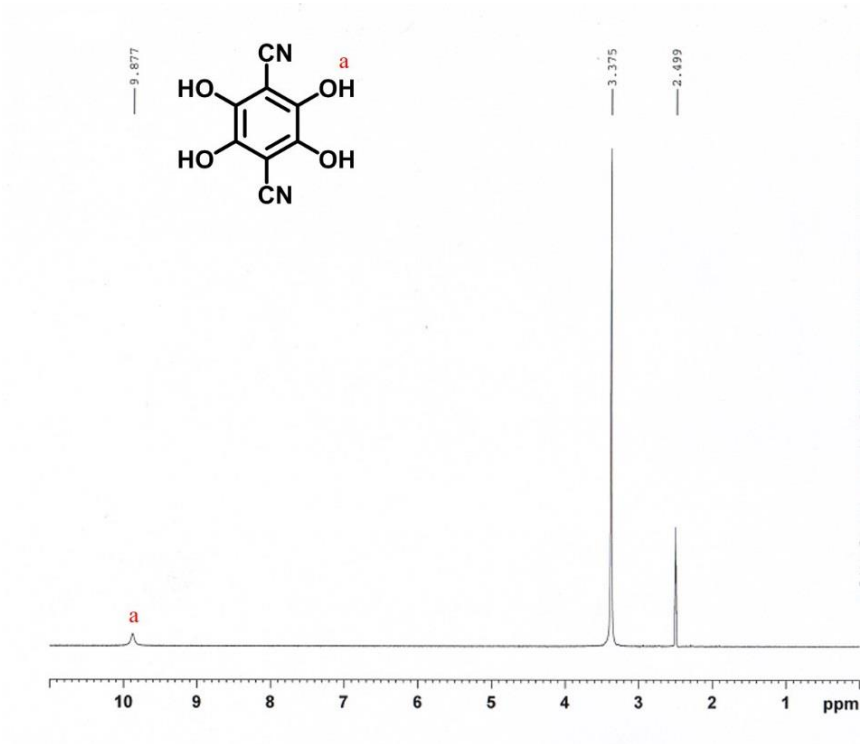

Fig. S3 ^{1}H NMR spectrum of LH_4.

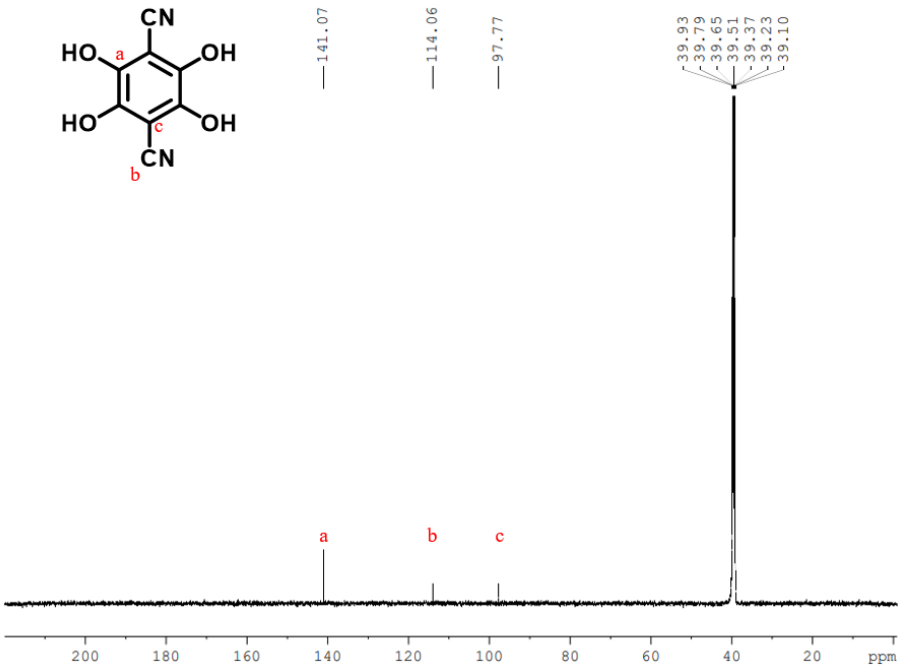

Fig. S4 ^{13}C NMR spectrum of LH_4.

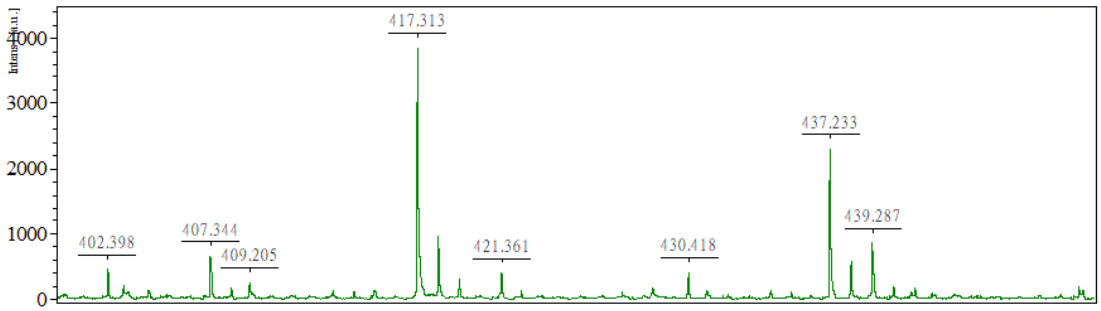

Fig. S5 Mass spectrum of 2, 3, 5, 6-tetra-*tert*-butoxyterephthalonitrile.

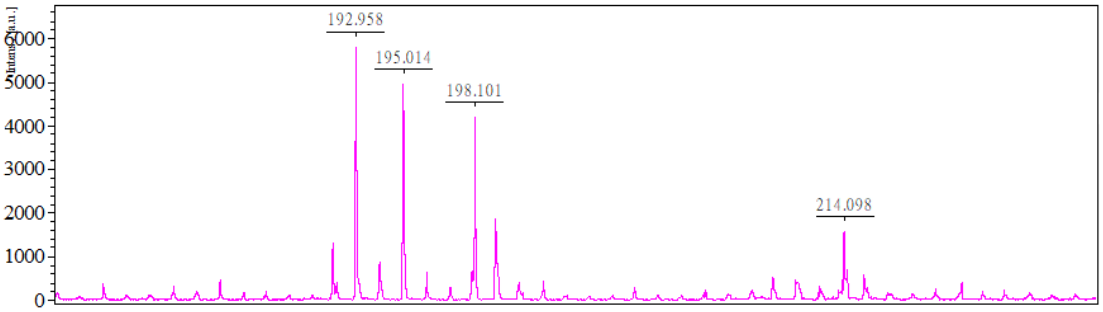

Fig. S6 Mass spectrum of LH_4.

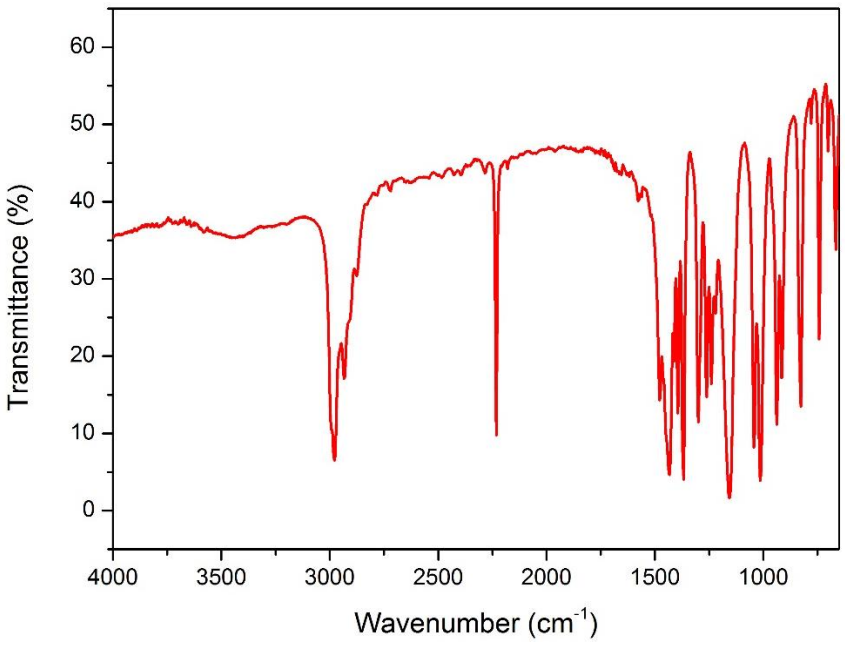

Fig. S7 FT-IR spectrum of 2, 3, 5, 6-tetra-*tert*-butoxyterephthalonitrile.

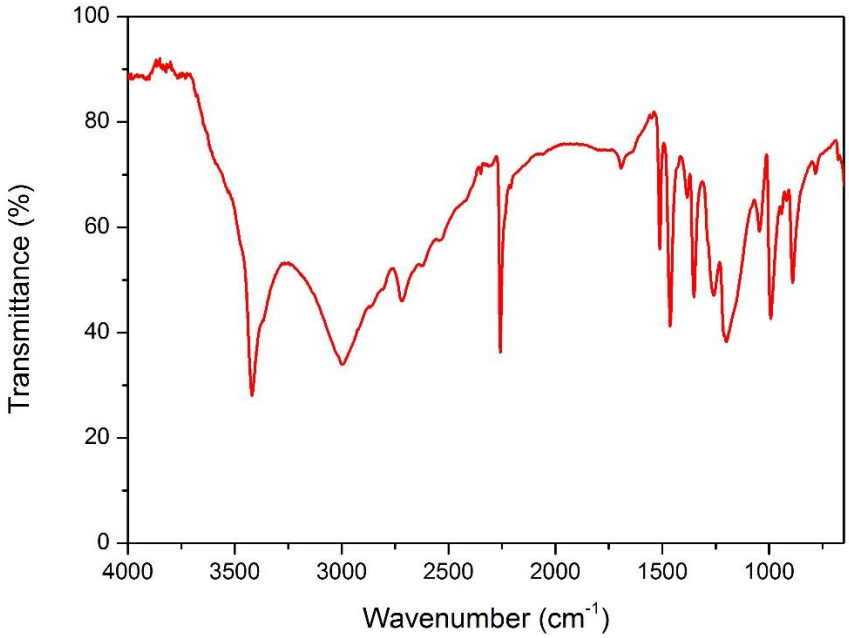

Fig. S8 FT-IR spectrum of LH_4.

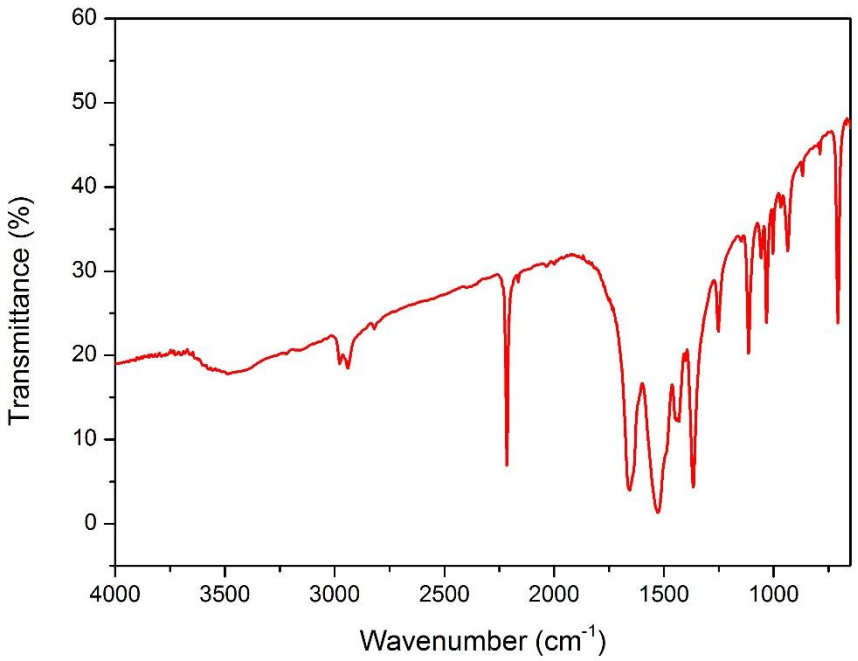

Fig. S9 FT-IR spectrum of $[CuL(DMF)_2]_n$.

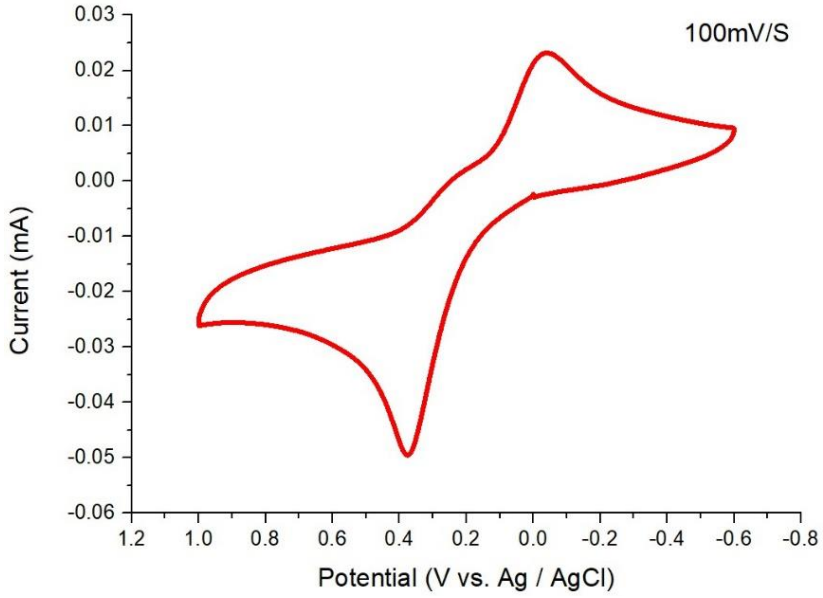

Fig. S10 CV plot of LH_4.

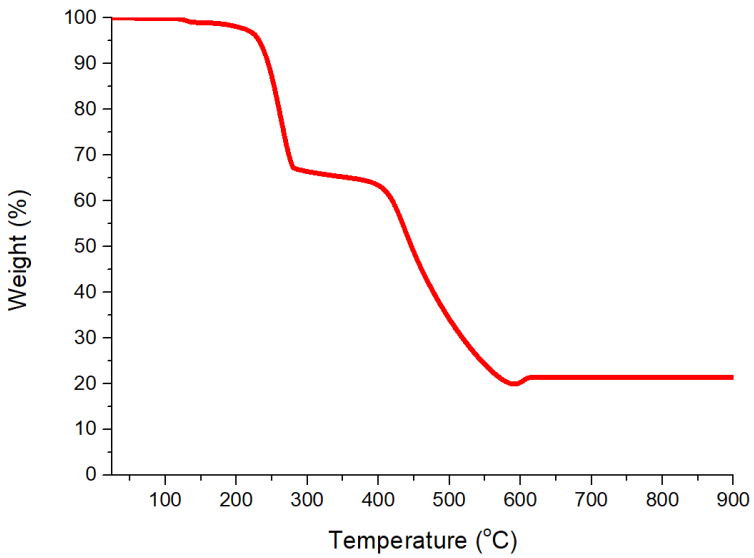

Fig. S11 TGA trace of $[CuL(DMF)_2]_n$.

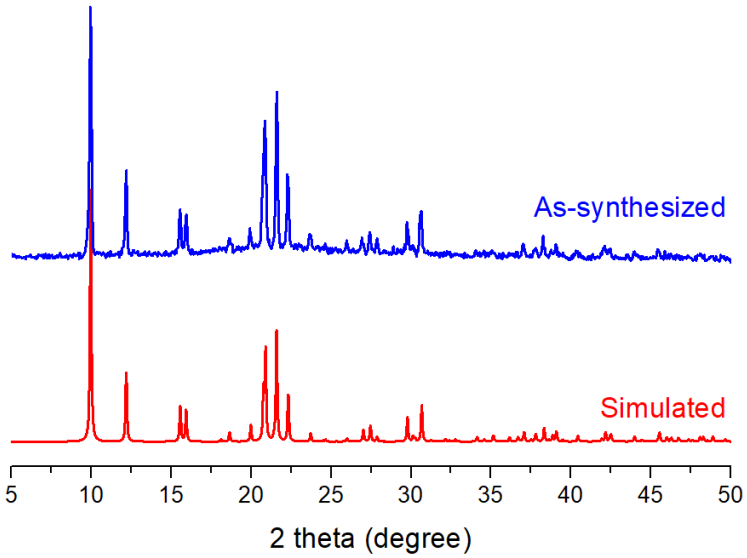

Fig. S12 PXRD patterns of $[CuL(DMF)_2]_n$.

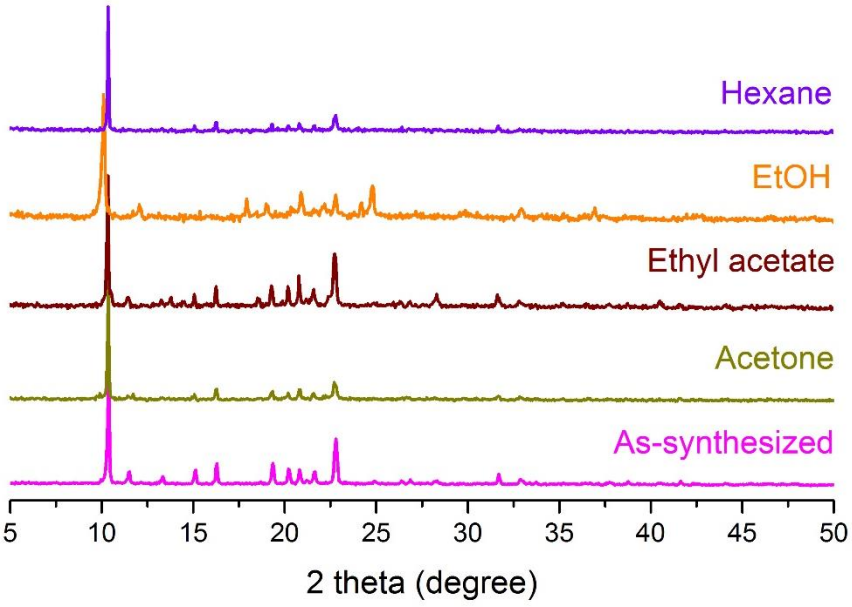

Fig. S13 PXRD patterns of $[CuL(DMF)_2]_n$ soaked in different solvents.

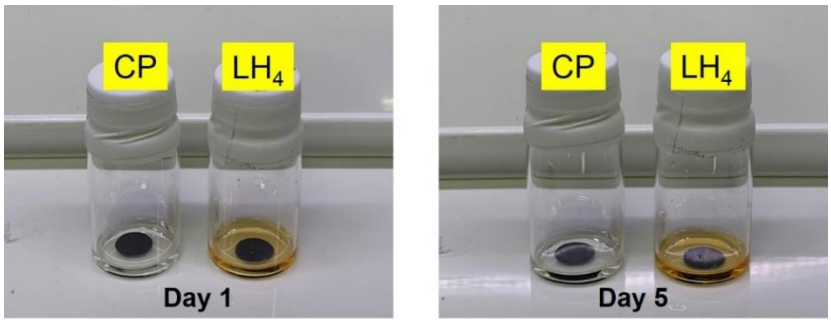

Fig. S14 Dissolution test of CP and LH_4 in electrolyte solution after 1 d (left) and 5 d (right).

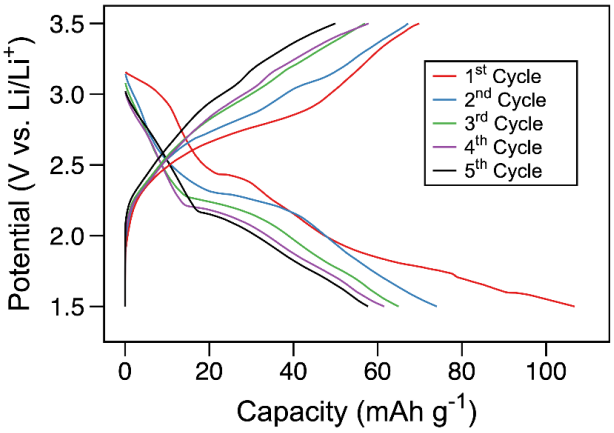

Fig. S15 Discharge-charge profiles of LH_4 at 10 mA g^{-1} for the first 5 cycles using 1 M $LiPF_6$ in EC/DMC (1:1) as electrolyte (LH_4 : Super P : KS4 : PVDF = 5:3:1:1).

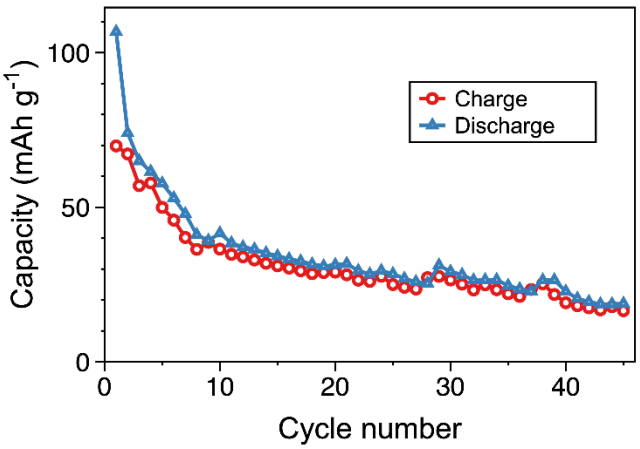

Fig. S16 Capacity retention of LH_4 at 10 mA g^{-1} (~C/14).

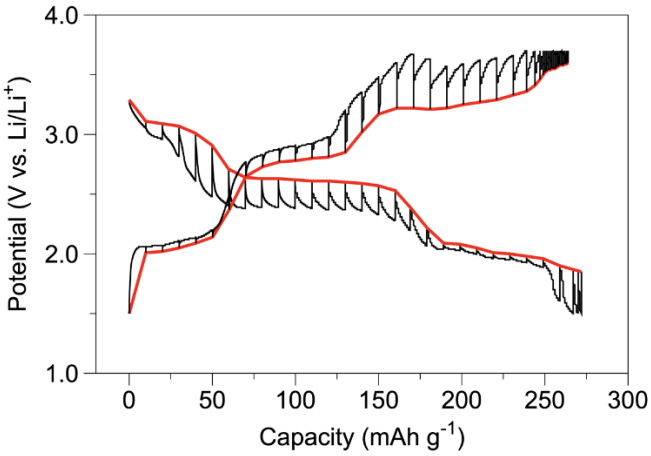

Fig. S17 GITT discharge/charge curves of $[CuL(DMF)_2]_n$. GITT is used to determine quasi-equilibrium potentials at different stages during cell cycling. Red curve is constructed from the last data point of each relaxation period. It has been observed that there is an overpotential of up to 300 mV on discharge and a comparable polarization (~200 mV) on charge, which suggests a kinetic limitation of the electrochemical reactions of the CP.

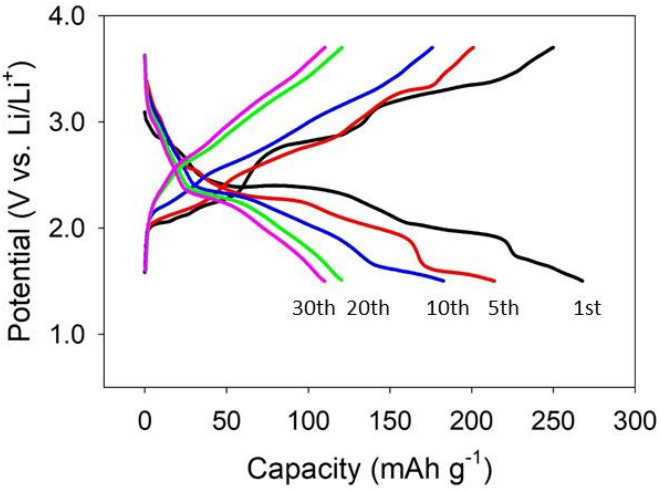

Fig. S18 Discharge/charge profiles of $[CuL(DMF)_2]_n$ with a rate of 80 mA g^{-1} at different cycles.

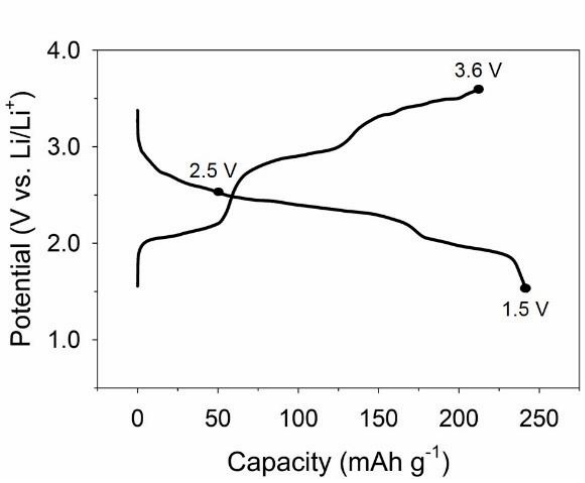

Fig. S19 Discharge-charge profile of CP electrode, labeled with different voltage positions for FT-IR and PXRD experiments.

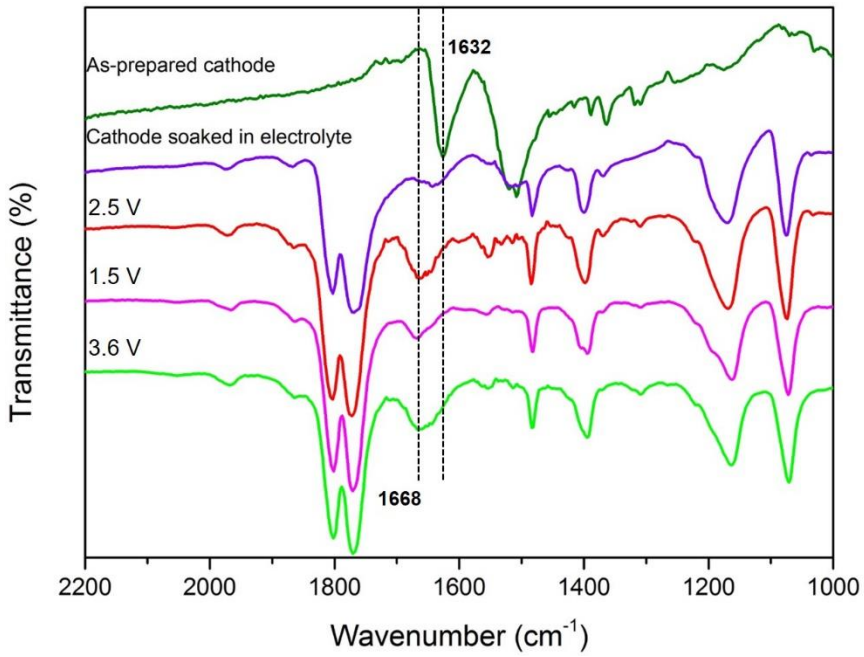

Fig. S20 FT-IR spectra of CP electrodes at different voltage positions. The coordinating carbonyl groups were observed at 1632 cm^{-1} (as-prepared cathode) and at 1668 cm^{-1} (discharged and charged electrodes).[1] The relative intensity of the carbonyl group decreased on discharge down to 1.5 V, and increased on charge up to 3.6 V.

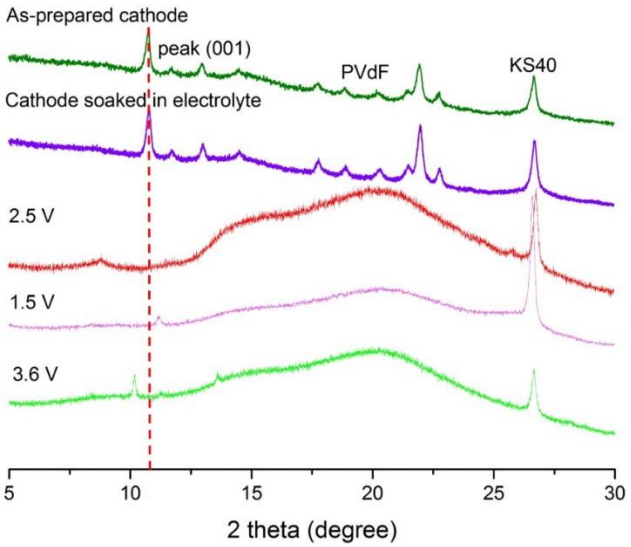

Fig. S21 *Ex situ* PXRD patterns of CP electrodes. The (001) peak of CP active material was obviously shifted during discharge-charge cycle. This result suggested the structural flexibility of CP.

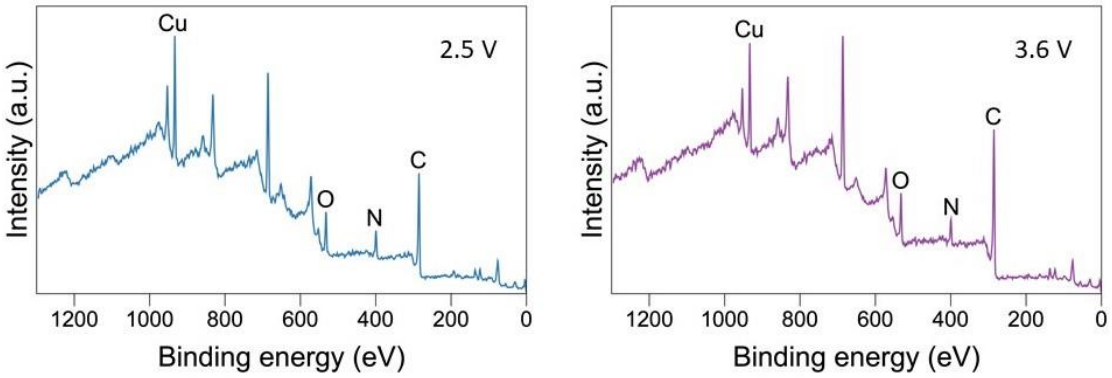

Fig. S22 XPS low-resolution survey data of CP electrodes at 2.5 and 3.6 V.

Extended X-ray absorption fine structure (EXAFS) analysis

EXAFS analysis of CP electrodes were carried out at Beamline TPS44A in National Synchrotron Radiation Research Center, Hsinchu, Taiwan. The Cu K-edge EXAFS spectra were collected in transmission mode, using nitrogen-filled gridded ionization chambers[2] with a quick-scanning monochromator at room temperature[3]. The parameters of the local structure around the copper atom were determined by curve-fitting procedures using Artemis[4] data analysis software.

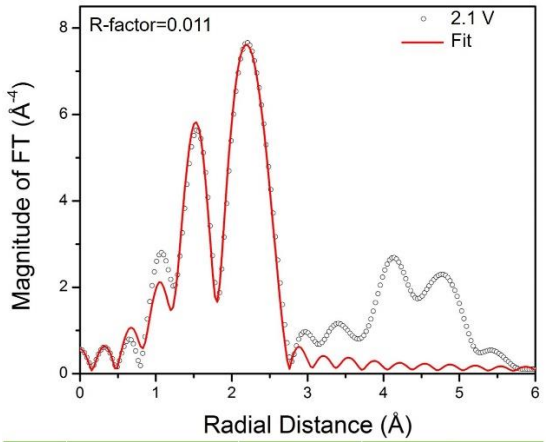

Path	N (coordination number)	L (bond length Å)	σ^2 (Debye-Waller factor Å^2)
Cu-O	1.45	1.92	0.003
Cu-Cu	3.03	2.53	0.008

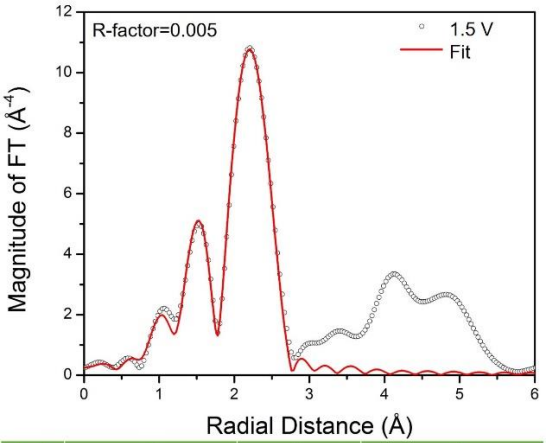

Path	N (coordination number)	L (bond length Å)	σ^2 (Debye-Waller factor Å^2)
Cu-O	1.12	1.90	0.003
Cu-Cu	4.42	2.53	0.009

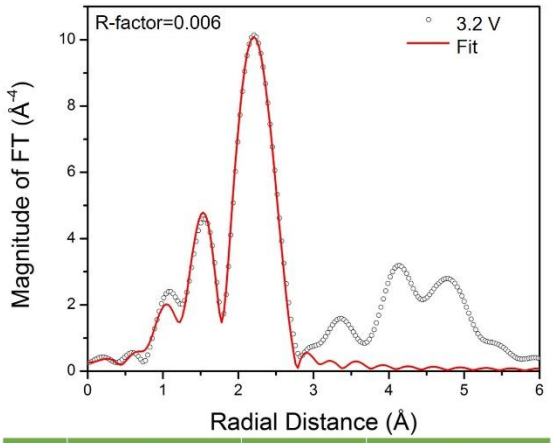

Path	N (coordination number)	L (bond length Å)	σ^2 (Debye-Waller factor Å^2)
Cu-O	1.18	1.91	0.004
Cu-Cu	4.08	2.54	0.008

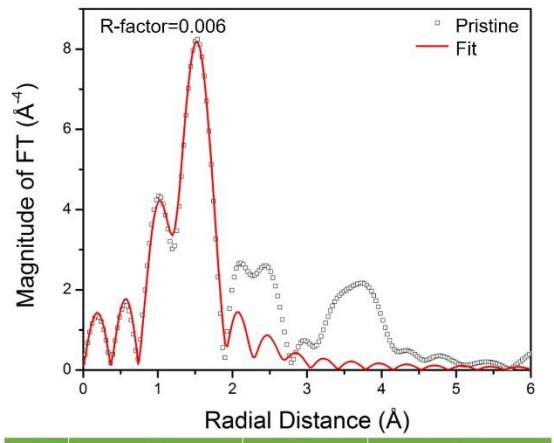

Path	N (coordination number)	L (bond length Å)	σ^2 (Debye-Waller factor Å^2)
Cu-O	3.05	1.94	0.006

Fig. S23 Cu K-edge EXAFS spectra of CP electrodes. The circle curves are the observed data and the solid lines are the best fit from the parameters in the corresponding tables.

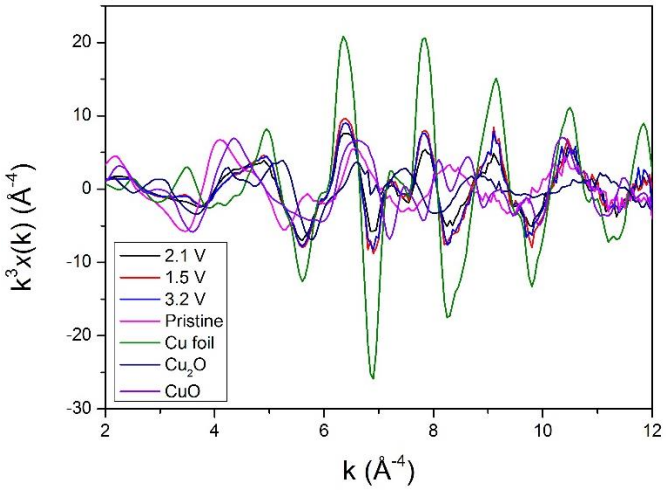

Fig. S24 Fourier-transformed $k^3\chi(k)$ vs. k EXAFS spectrum for CP electrodes.

Table S1. Crystallographic data for $[CuL(DMF)_2]_n$.

Identification code	d20140
Empirical formula	$C_{14}H_{14}CuN_4O_6$
Formula weight	397.83
Temperature/K	200(2)
Crystal system	Triclinic
Space group	$P\overline{1}$
a/Å	6.000(2)
b/Å	7.988(3)
c/Å	8.967(4)
α/°	75.720(14)
β/°	76.573(14)
γ/°	88.048(12)
Volume/Å^3	405.0(3)
Z	1
ρ_{calc} g/cm^3	1.631
μ/mm^{-1}	1.388
F(000)	203
Radiation	Mo Kα (λ = 0.71073)

2θ range for data collection/°	2.63 to 25.07
Index ranges	$-7 \leq h \leq 7$, $-9 \leq k \leq 9$, $-10 \leq l \leq 10$
Reflections collected	8086
Independent reflections	1416 [R_{int} = 0.0421, R_{sigma} = 0.0278]
Data/restraints/parameters	1416/0/117
Goodness-of-fit on F^2	1.092
Final R indexes [$I > 2\sigma(I)$]	R_1 = 0.0237, wR_2 = 0.0595
Final R indexes [all data]	R_1 = 0.0255, wR_2 = 0.0605
Largest diff. peak/hole / e Å^{-3}	0.27/-0.29

Table S2. Comprehensive overview of coordination polymers applied as cathode materials in Li-ion batteries.

Coordination polymer, dimension	Electrode composition (active material/conducting additive/binder)	Conducting additive	Binder	Theoretical capacity [mAh g^{-1}], 1st cycle, % material activity	Number of cycles, capacity last cycle [mAh g^{-1}], % material activity, current density	Charge voltage [V]	Discharge voltage [V]	Electrolyte	Reference
$[CuL(DMF)_2]_n$ 1D	30/60/10	Super P/ graphite KS4	PVDF	268, 268, 100	33, 120, 45, 80 mA g^{-1}	2.2, 2.8, 3.4	2.8, 2.4, 1.9	EC/DMC 1/1, 1M $LiPF_6$	This work
$[FePcOC(tz)]_n$ 1D	65/20/15	AB	PVDF	n.d., 1095, n.d.	100, 70, 6.4, 70 µA cm^{-2}	–	2.46	PC/DMC, 1M $LiPF_6$	5
$[FePcOC(dib)]_n$ 1D	60/25/15	AB	PVDF	n.d, 147, n.d.	60, 147, 100, 70 µA cm^{-2}	–	3.2	DME 1M $LiPF_6$	6
$[Li_2(C_6H_2O_4)]$ 1D	60/35/5	AB	PTFE	n.d., 176, n.d.	10, 137, 78%, 100 mA g^{-1}	2.3	2.1	EC/DMC 1/1, 1M $LiPF_6$	7
$Li_2PDHBQS$ 1D	60/30/10	CC	PTFE	295, 285, 97%	1500, 239, 89%, 500 mA g^{-1}	2.0	2.0	DOL/DME 1/1, 1M $LiN(CF_3SO_2)_2$	8
CuTIB 2D	40/50/10	Super P	PVDF	n.d., 155, n.d.	150, 50, 32%, 50 mA g^{-1}	–	–	EC/DMC 1/1, 1M $LiPF_6$	9
$\{[Cd(ClO_4)_2(DPNDI)_2]\cdot(DMA)_{4.5}\cdot(H_2O)_2\}_n$, 2D	45/45/10	Super P	PVDF	n.d., 46.8, n.d.	50, 36.7, 78.4%, 100 mA g^{-1}	–	2.6–2.3	EC/EMC/DMC 1/1/1, 1M $LiPF_6$	10
$Cu_3(HHTP)_2$ 2D	80/0/20	None	PVDF	95.6, 95, 99%	20, 94.9, 99%, 1C	2.55	2.55	EC/DMC 1/1 1M $LiPF_6$	11

Coordination polymer, dimension	Electrode composition (active material/conducting additive/binder)	Conducting additive	Binder	Theoretical capacity [mAh g^{-1}], 1st cycle, % material activity	Number of cycles, capacity last cycle [mAh g^{-1}], % material activity, current density	Charge voltage [V]	Discharge voltage [V]	Electrolyte	Reference
MIL-101(Fe) 3D	33/33/33	KB	PTFE	n.d., 60, n.d.	100, 72, 1.2, 0.2 C	2.6	3.2	EC/DMC 1/2 1M $LiPF_6$	12
MIL-53(Fe)·H_2O 3D	85/15/0	Super P	None	n.d., 80, n.d.	50, 75, 94%, C/40	–	2.9V	EC/DMC 1/1 1M $LiPF_6$	13
Cu(2,7-AQDC) 3D	10/70/20	CB	PVDF	162, 147, 91%	50, 105, 65%, 1 mA g^{-1}	–	3.2–2.4 2.4–1.7	EC/DEC 1/1 1M $LiPF_6$	14
Mn_7(2,7-AQDC)$_6$(2,6-AQDC) $(DMA)_6$, 3D	10/70/20	CB	PVDF	190, 205, 108%	50, 177, 93%, 1 mA g^{-1}	–	3.2	EC/DEC 1/1 1M $LiPF_6$	15
Cu-TCA 3D	80/10/10	Super P	PVDF	145, 102.2, 70%	200, 39.9, 39%, 0.5 C	2.9–3.5 3.8–4.3	4.3–3.9 2–1.8	EC/DMC 1/1 1M $LiPF_6$	16
$\{CoLi(BTC)(DMA)_2\}_n$ 3D	60/30/10	AB	PVDF	n.d., 156, n.d.	50, 64, 41%, 50 mA g^{-1}	–	–	EC/DEC/EMC 1/1/1, 1M $LiPF_6$	17
V^{IV}(O)(bdc) 3D	65/30/5	AB	PVDF	n.d., 118, n.d.	50, 82, 69%, 10 mA g^{-1}	–	2.7	EC/DMC 1/1 1M $LiPF_6$	18
CuFe-PBA@NiFe-PBA, 3D	70/15/15	AB	PTFE	n.d., 99, n.d.	50, 64, 65%, 10 mA g^{-1}	–	3.24, 2.95	EC/DEC 1/1 1M $LiPF_6$	19
$K_2Mn[Mn(CN)_6]$ 3D	75/20/5	AB	PTFE	176, 197, 112%	10, 140, 71%, 30 mA g^{-1}	3.7, 3.0	3.7, 3.0	EC/DEC 1/1 1M $LiPF_6$	20
FeHCCo 3D	70/20/10	Super P	PVDF	n.d., 136, n.d.	40, 150, 110%, 0.63 C	–	–	EC/DEC 1/1 1M $LiPF_6$	21

n.d.; not determined, PVDF: poly(vinylidene fluoride), EC: ethylene carbonate, DMC: dimethyl carbonate, PcOC: octacyanophthalocyanine, tz: tetrazine, AB: acetylene black, PC: propylene carbonate, dib: diisocyanobenzene, DME: dimethoxyethane, PTFE: polytetrafluoroethylene, PDHBQS: 2,5-dihydroxy-*p*-benzoquinonyl sulfide, CC: conductive carbon, DOL: 1,3-dioxolane, TIB: 1,2,4,5-tetraaminobenzene, DPNDI: *N,N'*-di(4-pyridyl)-1,4,5,8-naphthalenediimide, EMC: ethylene methyl carbonate, DMA: N,N-dimethylacetamide, HHTP: 2,3,6,7,10,11-hexahydroxytriphenylene, KB; Ketjen black, 2,7-AQDC: 2,7-anthraquinonedicarboxylate, 2,6-AQDC: 2,6-anthraquinonedicarboxylate, TCA: tricarboxytriphenyl amine, BTC: 1,3,5-benzenetricarboxylate, bdc: 1,4-benzenedicarboxylate, PBA: prussian blue analogues, HCCo: hexacyanocobaltate.

References

1. B. Cheng, H. Yi, C. He, C. Liu and A. Lei, *Organometallics*, 2015, **34**, 206–211.
2. O. Müller, J. Stötzel, D. Lützenkirchen-Hecht and R. Frahm, *J. Phys. Conf. Ser.* 2013, **425**, 092010.
3. O. Müller, D. Lützenkirchen-Hecht and R. Frahm, *Rev. Sci. Instrum.* 2015, **86**, 093905.
4. B. Ravel and M. Newville, *J. Synchrotron. Rad.* 2005, **12**, 537–541.
5. S.-J. Kim, K. Onishi, M. Matsumoto and K. Shigehara, *J. Porphyrins Phthalocyanines,* 2001, **5**, 397–404.
6. Y. Asai, K. Onishi, S. Miyata, S.-J. Kim, M. Matsumoto and K. Shigehara, *J. Electrochem. Soc.*, 2001, **148**, A305–A310.
7. J. Xiang, C. Chang, M. Li, S. Wu, L. Yuan and J. Sun, *Cryst. Growth Des.*, 2008, **8**, 280–282.
8. Z. Song, Y. Qian, X. Liu, T. Zhang, Y. Zhu, H. Yu, M. Otani and H. Zhou, *Energy Environ. Sci.*, 2014, **7**, 4077–4086.
9. R. R. Kapaev, S. Olthof, I. S. Zhidkov, E. Z. Kurmaev, K. J. Stevenson, K. Meerholz and P. A. Troshin, *Chem. Mater.*, 2019, doi: 10.1021/acs.chemmater.9b01366.
10. B. Tian, G.-H. Ning, Q. Gao, L.-M. Tan, W. Tang, Z. Chen, C. Su and K. P. Loh, *ACS Appl. Mater. Interfaces*, 2016, **8**, 31067–31075.
11. S. Gu, Z. Bai, S. Majumder, B. Huang, G. Chen, *J. Power Sources*, 2019, **429**, 22–29.
12. T. Yamada, K. Shiraishi, H. Kitagawa and N. Kimizuka, *Chem. Commun.*, 2017, **53**, 8215–8218.
13. G. Férey, F. Millange, M. Morcrette, C. Serre, M.-L. Doublet, J.-M. Grenèche and J.-M. Tarascon, *Angew. Chem. Int. Ed.,* 2007, **46**, 3259–3263.
14. Z. Zhang, H. Yoshikawa and K. Awaga, *J. Am. Chem. Soc.*, 2014, **136**, 16112–16115.
15. Z. Zhang, H. Yoshikawa and K. Awaga, *Chem. Mater.*, 2016, **28**, 1298–1303.
16. Z. Peng, X. Yi, Z. Liu, J. Shang and D. Wang, *ACS Appl. Mater. Interfaces*, 2016, **8**, 14578–14585.
17. Z.-Q. Du, Y.-P. Li, X.-X. Wang, J. Wang and Q.-G. Zhai, *Dalton Trans.*, 2019, **48**, 2013–2018.
18. W. Kaveevivitchai and A. J. Jacobson, *J. Power Sources*, 2015, **278**, 265–273.
19. D. Asakura, C. H. Li, Y. Mizuno, M. Okubo, H. Zhou and D. R. Talham, *J. Am.*

Chem. Soc., 2013, **135**, 2793–2799.

20. D. Asakura, M. Okubo, Y. Mizuno, T. Kudo, H. Zhou, K. Ikedo, T. Mizokawa, A. Okazawa and N. Kojima, *J. Phys. Chem. C*, 2012, **116**, 8364–8369.
21. K. Zhang, R. S. Varma, H. W. Jang, J.-W. Choi and M. Shokouhimehr, *J. Alloys Compd*, 2012, **791**, 911–917.